

# Real-Time Magnetic Field Sensing based on Microwave Frequency Modulated Photocurrent of Nitrogen-Vacancy Centers in Diamond

Xuan-Ming Shen<sup>1†</sup>, Qilong Wu<sup>1†</sup>, Huihui Yu<sup>1†</sup>, Pei-Nan Ni<sup>1</sup>, Qing Lou<sup>1</sup>, Chao-Nan Lin<sup>2</sup>, Xun Yang<sup>1\*</sup>, Chong-Xin Shan<sup>1\*</sup>, Yuan Zhang<sup>1,2\*</sup>

1. Henan Key Laboratory of Diamond Materials and Devices, Key Laboratory of Material Physics, Ministry of Education, School of Physics, Zhengzhou University, Zhengzhou 450052, China

2. Institute of Quantum Materials and Physics, Henan Academy of Sciences, Zhengzhou 450046, China

While photoelectric detection of magnetic resonance (PDMR) can be applied to miniaturize nitrogen-vacancy (NV) center-based quantum sensors, the real demonstration of PDMR-based magnetic field sensing remains as a distinctive challenge. To tackle this challenge, in this article, we fabricate diamond samples with electrodes and microwave antenna on the surface, and realize PDMR by detecting photocurrent in nanoampere range via various lock-in amplifying modes. Importantly, we obtain a theoretical and experimental sensitivity  $397 \text{ nT}/\sqrt{\text{Hz}}$  and  $921 \text{ nT}/\sqrt{\text{Hz}}$  of magnetic field detection in DC~10 Hz range with a laser intensity and microwave frequency modulated mode, respectively, and demonstrate for the first time, a real-time tracking of alternating magnetic field with a standard deviation of  $1.5 \mu\text{T}$ . Furthermore, we investigate systematically the dependence of the PDMR contrast, linewidth and the sensitivity on the laser and microwave power, and find a perfect agreement with a master equation based theoretical model, which accounts for not only the optically induced charge switch of neutral and negative NV centers, but also the interaction with microwave field.

## I. INTRODUCTION

Nitrogen-vacancy (NV) center as a prototype solid-state qubit has attracted considerable attention in the fields of quantum information [1,2], quantum computation [3-5] and quantum sensing [6-8], owing to its long spin coherence time at room temperature [9,10], convenient spin initialization and readout with optical means. Beyond the conventional readout via spin-dependent photoluminescence, other readout schemes have also been actively investigated in recent years, including the readout via photocurrent [11], infrared absorption [12], and microwave transmission [13]. Among these schemes, electrical readout as explored in electrical/photocurrent detection of magnetic resonance (EDMR/PDMR) technique attracts

particular interest [11,14,15], as it removes the requirement of optics to collect the NV center fluorescence, and bulky photon-detectors to convert the fluorescence to electric signal [16-19], which thereby can facilitate the integration and miniaturization of the NV center-based quantum sensors [20].

The development of PDMR has followed the path of the photon readout scheme, achieving the milestones of detecting NV spin ensembles [15,21,22], single NV spins [23,24], and nuclear spins [25,26]. All these are enabled by a better understanding of the laser-induced charge switch of negative and neutral NV centers [27]. While PDMR-based magnetic detection has been reported before [20,28,29], these studies employ mainly lock-in amplifier (LIA) with either laser or microwave modulation to detect the weak

---

\*yzhuanidpc@zzu.edu.cn

photocurrent and to obtain the PDMR spectra, and estimate theoretically the magnetic field sensitivity through theoretical formulas. In addition, although PDMR was also demonstrated recently with other color centers [30-32], the corresponding magnetic field sensing still lacks a systematic characterization and thorough validation. Thus, to further advance PDMR technology and its practical applications, it is essential to develop LIA techniques based on *microwave frequency modulation* to achieve a dispersive PDMR spectrum, to validate the theoretically calculated magnetic field sensitivity with amplitude spectral density measurement, and to demonstrate real-time magnetic field sensing under practical conditions.

To address the above challenges, in the present article, we investigate the PDMR based magnetic field sensing by fabricating a diamond sample with integrated electrodes and microwave antennas on the surface, and detecting weak photocurrent in nanoampere range via various lock-in amplifying modes [33]. We obtain a theoretically estimated and experimentally validated sensitivity of 397 nT/ $\sqrt{\text{Hz}}$  and 921 nT/ $\sqrt{\text{Hz}}$  for magnetic field detection with a laser intensity and microwave frequency modulated mode, respectively, and demonstrate for the first time, a real-time magnetic field sensing with a standard deviation of 1.5  $\mu\text{T}$ . Importantly, we carry out a systematic study of the dependence of the PDMR contrast, linewidth and the sensitivity on the laser and microwave power, and achieve a perfect agreement with a master equation based theoretical model, which accounts for not only the charge switch of negative and neutral NV centers, but also the interaction with a microwave radiation. Based on this agreement, we further estimate that the magnetic field sensitivity might be improved to tens nT/ $\sqrt{\text{Hz}}$  by using a diamond sample featuring stronger NV concentration.

## II. NV CENTER AND EXPERIMENTAL

## SETUP

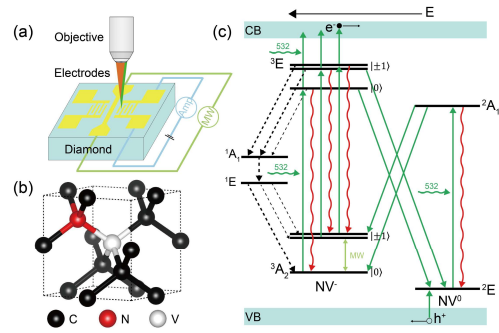


FIG. 1. Setup and operating principles. (a) Simplified diagram of the setup, where a 532 nm laser is focused between two electrodes and near a microwave antenna on a MPCVD diamond sample, and the photocurrent is detected through a lock-in amplifier. (b) Atomic structure of NV centers, where black, red and white spheres represent carbon atoms, nitrogen atom and vacancy, respectively. (c) Energy level diagram and rich processes of negatively charged (NV<sup>-</sup>) and neutral NV centers (NV<sup>0</sup>), where laser excitation (green arrows) leads to the fluorescence (red arrows) and the generation of electrons in conduction band (CB) and holes in valence band (VB) through charge-state conversion. For more information see the text.

Figure 1(a) shows the simplified schematic of the setup and the sample, which are further detailed in Section S1 and S2 of the Supplemental Material (SM). The sample is a MPCVD diamond grown in our lab, and features two pairs of interdigitated gold electrodes and a gold microbelt as a microwave antenna on the surface. A 532 nm laser is focused between two gold electrodes through an objective, and the NV fluorescence is detected in an inverted direction. The microwave is first amplified, and then delivered through the antenna near the electrodes. A DC voltage is applied between the electrodes, and the photocurrent is detected with a lock-in amplifier.

NV center is a point defect formed by a substitutional nitrogen atom and an adjacent

vacancy in the diamond crystal [Fig. 1(b)]. NV center can be either in a neutral form ( $\text{NV}^0$ ) or a negatively charged form ( $\text{NV}^-$ ), where  $\text{NV}^-$  has a triplet ground and excited state  $^3\text{A}_2$ ,  $^3\text{E}$  and two singlet excited states  $^1\text{A}_1$  and  $^1\text{E}$ , and  $\text{NV}^0$  has a doublet ground state  $^2\text{E}$  and excited state  $^2\text{A}_1$  [Fig. 1(c)]. In addition, the fine structure of triplet states can be labeled by magnetic projection numbers  $m_s = 0, \pm 1$ , and the degenerate  $m_s = \pm 1$  states are about 2.87 GHz and 1.42 GHz above the  $m_s = 0$  state for the  $^3\text{A}_2$  and  $^3\text{E}$  state.

Under 532 nm laser illumination, the  $\text{NV}^-$  can be excited to the  $^3\text{E}$  state and then be converted to  $\text{NV}^0$  by absorbing one photon and two photons, leaving a free electron in the conduction band of diamond. Similarly,  $\text{NV}^0$  can be excited to the  $^2\text{A}_1$  state and then converted to  $\text{NV}^-$  by absorbing one and two photons, generating a free hole in the valence band of diamond. The excited  $\text{NV}^-$  and  $\text{NV}^0$  can decay to the ground state through spontaneous emission, while the excited  $\text{NV}^-$  can also decay through non-radiative processes involving triplet-singlet intersystem crossing (ISC) and the decay from the  $^1\text{A}_1$  state to the  $^1\text{E}$  state. Because the ISC rate from the  $^3\text{A}_2$ ,  $m_s = \pm 1$  states is faster than that from the  $^3\text{A}_2$ ,  $m_s = 0$  state in the  $\text{NV}^-$  center, the non-radiative process leads to large population on the  $m_s = 0$  state, and also results in a spin-dependent photocurrent and fluorescence. When a microwave at around 2.87 GHz is applied to the NV centers, the population is transferred from the  $^3\text{A}_2$ ,  $m_s = 0$  level to the  $^3\text{A}_2$ ,  $m_s = \pm 1$  level, and the corresponding photocurrent and fluorescence will be reduced, forming the principles behind PDMR and Optical Detection of Magnetic Resonance (ODMR). In the presence of a weak magnetic field, the  $m_s = +1$  and  $m_s = -1$  levels can be shifted slightly upwards and downwards in energy, respectively, and the PDMR and ODMR spectra become modified, from which the magnetic field can be inferred.

In many studies on PDMR and ODMR,

lock-in amplifier is often adopted to extract the signal from the noisy photocurrent or fluorescence, where the laser intensity [15, 28], the microwave intensity and frequency [17, 34-36] or even the external magnetic field can be modulated. Among these modes, microwave frequency-modulation is often adopted to implement the ODMR based real-time detection of alternating magnetic field, since the resulting dispersive spectrum shows a linear scaling of the lock-in output to the microwave carrier frequency under resonant condition, and thus the lock-in output can be directly converted to the measured magnetic field [32,37]. However, as far as we know, such a technique has not been explored in the studies of PDMR, and thus there is no report so far on the PDMR based real-time magnetic field detection.

### III. EXPERIMENTAL AND THEORETICAL RESULTS

In this section, the photocurrent-voltage and photocurrent-laser power measurement on the diamond samples with NV centers were characterized firstly. Then, the lock-in PDMR with the laser intensity modulation was presented, and the expected sensitivity of the magnetic field detection was estimated theoretically. After that, the lock-in PDMR with the microwave frequency modulation was discussed, and the theoretical sensitivity was verified through the amplitude spectral density measurement, as well as the real-time tracking of alternative magnetic field was demonstrated. Finally, the dependence of the system performance was studied on the laser and microwave power, and the experimental results were compared with master equation based theoretical data.

#### A. Photocurrent-Voltage and -Laser Power Characteristics

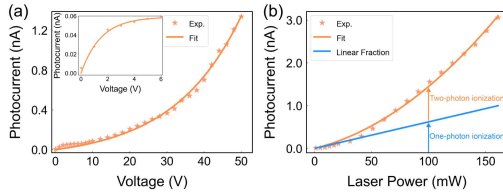


FIG. 2. Electric characterization of the NV center diamond sample. (a) Photocurrent as function of the applied DC voltage for given laser power 100 mW (the inset presents the magnified results in the voltage range of 0–6 V), (b) Photocurrent as function of the laser power for an applied voltage of 50 V. The experimental data (orange star) are fitted with nonlinear functions stated in the main text (orange curves). In panel (b), the blue curve is the linear fraction of the photocurrent.

In the experiment, we firstly characterize the built device with the photocurrent-voltage (I-V) and the photocurrent-laser power (I-P) curves [Figs. 2a, 2b]. To this end, we apply a DC voltage and a continuous laser illumination on the device, and setup the low-noise current amplifier with a low-pass filter cut-off frequency of 0.03 Hz and a proper transimpedance gain of 1 nA/V, and then average the DC photocurrent with the oscilloscope integrated in the LIA for 5 s.

Figure 2(a) illustrates the I-V characteristics for 100 mW laser illumination, which shows a raising and saturated trend in the low voltage range (inset) and an exponentially increased behavior in the high voltage range. Inspired by our previous study [38] and a recent study [39], we realize that the electrode-diamond-electrode structure in our device forms two back-to-back connected Schottky junctions. At low voltage, the current is determined by the backward biased junction, and follows the expression  $J_1 = A_1(1 - e^{-U/U_1})$ . At high voltage, the depletion region of this junction increases and touches that of another junction. As a result, the two junctions merge as single Schottky junction, and the current is determined by the forward biased expression  $J_2 = A_2(e^{U/U_2} - 1)$ . Using the two expressions to fit the I-V curve in the low- and high voltage

range, we obtain the amplitudes  $A_1 = 59.1 \pm 2.3$  pA,  $A_2 = 93.31 \pm 7.1$  pA, and the saturated and threshold voltage  $U_1 = 1.5$  V,  $U_2 = 18.28$  V. Since the large photocurrent under high bias can be more easily detected with the LIA, a DC bias voltage of 50 V is used for subsequent measurements.

Figure 2(b) shows that the photocurrent  $J$  increases firstly slowly with the laser power  $P$  for weak laser illumination, but much faster for the laser power exceeding 50 mW. Since the optically induced carriers from the NV centers originate from two-photons ionization of  $\text{NV}^-$  and two-photons recombination of  $\text{NV}^0$ , the photocurrent is expected to scale quadratically with the laser power. However, due to the presence of other photon-active defects in the diamond, the photocurrent contains also a background contribution, which should scale linearly with the laser power. Thus, we fit the data in Fig. 2(b) with the expression  $J = aP + bP^2$  to obtain the fitting parameters  $a = 6.602$  pA/mW and  $b = 0.079$  pA/mW<sup>2</sup>. The laser power, where the linear term equals to the quadratic term, can be estimated as  $\frac{a}{b} \approx 86$  mW.

Thus, in the following study, we utilize the laser power of 100 mW such that the photocurrent from the NV centers should dominate.

## B. Laser Intensity-modulated Lock-in PDMR

In the experiment shown in Fig. 3, the 100 mW laser beam was modulated by a 321 Hz square wave, and a DC voltage was applied between the electrodes. After amplifying the photocurrent by the pre-amplifier with a 0.3~1 kHz band-pass filter and a transimpedance gain of 1 nA/V, the output voltage was demodulated with LIA. By integrating the photocurrent of 4 s for the microwave near and far-detuned from 2.87 GHz with a power of 26 dBm, and then calculating their contrast, the PDMR spectrum was obtained, as shown by blue stars in Fig. 3(a). By fitting this curve with a Lorentzian function

$$L(f) = C \frac{(\Gamma/2)^2}{(f - f_0)^2 + (\Gamma/2)^2} + C_0, \quad (1)$$

a maximal contrast  $C = 12.1\%$ , a center frequency  $f_0 = 2869\text{MHz}$ , and a linewidth  $\Gamma = 19.5\text{ MHz}$  can be extracted. Then, the shot-noise limited sensitivity can be estimated according to the following expression [40]:

$$\eta_{SN} = \frac{4h}{3\sqrt{3}g\mu_B} \frac{\Gamma}{C\sqrt{R}}. \quad (2)$$

Here,  $h$  is Planck constant,  $g \approx 2.003$  is the electron  $g$  factor,  $\mu_B$  is the Bohr magneton, and  $R$  is the rate of photocarriers detection. Note that here  $R$  corresponds to the photocurrent detected with the LIA when the laser or microwave are modulated [see Fig. S5(e)], and it should not be confused with the photocurrent measured without modulation, as shown in Fig. 2(b). Using the fitted parameters, a magnetic field sensitivity of  $\eta_{SN} = 397\text{ nT}/\sqrt{\text{Hz}}$  can be estimated, as indicated by the blue dashed line in Fig. 3(c).

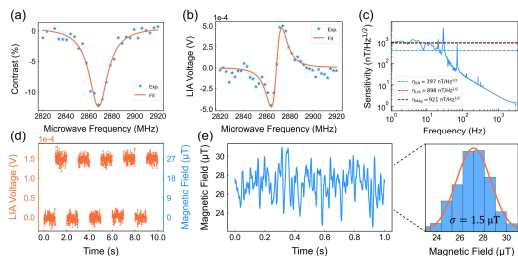


FIG. 3. PDMR and magnetic field sensing. (a) PDMR spectrum with the laser intensity modulation. (b) Lock-in voltage as function of the microwave frequency with microwave frequency-modulation. Blue stars are the experimental results, and the orange curves are the fits according to the expressions stated in the text. (c) Sensitivity of the magnetic field detection based on frequency-modulated PDMR as function of the frequency (blue noisy curve), and the corresponding theoretical estimations (dashed vertical lines). (d) Real-time tracking of an alternating magnetic field (right axis), as derived from the lock-in voltage (left axis). (e) Enlarged trace of the magnetic field signal from the final 1-second segment of (d) and the histogram of the magnetic field.

steady-state value with a standard deviation of  $1.5\text{ }\mu\text{T}$ . For the panels (a-e), the DC voltage is  $50\text{ V}$ , the laser power is  $100\text{ mW}$ , the microwave power is  $26\text{ dBm}$ , and the frequency-modulation depth is  $1\text{ MHz}$ . For more details, see the text.

### C. Microwave Frequency-modulated Lock-in PDMR

Since the above PDMR spectrum with a dip does not show a linear dependence on the microwave frequency, it is not convenient to utilize it for weak magnetic field sensing. To solve this problem, we explore the lock-in detection based on the microwave frequency-modulation, and obtain a PDMR spectrum with a dispersive shape as shown in Fig. 3(b), where the lock-in voltage shows a linear scaling with the microwave around  $2870\text{ MHz}$  frequency. By fitting the curve with the following expression [41]:

$$L(f) = -\frac{32}{3\sqrt{3}}C \frac{(f - f_0)\Gamma^3}{[4(f - f_0)^2 + \Gamma^2]^2}, \quad (3)$$

a maximal amplitude  $C = 5 \times 10^{-4}\text{ V}$ , a center frequency  $f_0 = 2868.43\text{ MHz}$ , a linewidth  $\Gamma = 15.257\text{ MHz}$  were obtained. For the linear region near the resonance,  $L \approx S(f - f_0) = S\gamma_e B$  with

$$a \text{ slope of } S = \frac{32\sqrt{3}C}{9\Gamma} = 2.018 \times 10^{-4}\text{ V/MHz}$$

were obtained. Here,  $\gamma_e = g\mu_B = 2.8\text{ MHz/Gauss}$  is the gyromagnetic ratio of the electron. The inversed expression  $B = L/(S\gamma_e)$  can be explored to infer the weak magnetic field in a real-time fashion. Then, the sensitivity of the magnetic field sensing can be theoretically estimated through the expression [42]

$$\eta_{LIA} = \frac{\sigma}{\gamma_e S \sqrt{2f_{ENBW}}} \quad (4)$$

as  $898\text{ nT}/\sqrt{\text{Hz}}$  [red dashed line in Fig. 3(c)] with the standard deviation of the LIA signal  $\sigma = 2.274 \times 10^{-5}\text{ V}$  and the equivalent noise bandwidth of the LIA  $f_{ENBW} = 10\text{ Hz}$ .

To verify experimentally the theoretically

estimated sensitivity, the lock-in voltage  $\{V_i\}$  was recorded under the resonance condition for 5 s, and was then translated to the magnetic field  $\{B_i\}$ . Then, the data was chopped into segments of  $\tau = 1$  s long, and discrete Fourier transform  $\mathcal{F}$  was performed to calculate the amplitude spectral density  $\frac{|\mathcal{F}|}{S\gamma_e}\sqrt{\tau}$  [33,34,43-45]. The obtained

spectrum is shown as the blue noisy curve in Fig. 3(c), and indicates a sensitivity of  $\eta_{Mag} \approx 921 \text{ nT}/\sqrt{\text{Hz}}$  (black dashed line) in the frequency range 1-10 Hz. Such a sensitivity is close to that estimated with Eq. (4), but is about 2 times smaller than that estimated with Eq. (2), which can be attributed to the electronic noise of the measurement setup.

By exploring the linear region in the microwave frequency-modulated PDMR, we can now demonstrate the real-time tracking of the magnetic field [Fig. 3(d)]. To this end, we place an electromagnet beside our setup, and modulate the applied magnetic field by changing the electromagnet current periodically with a frequency 1 Hz. An alternation of the lock-in voltage between 0.15 mV and 0 mV was observed, which corresponds to a magnetic field variation between 27  $\mu\text{T}$  and 0  $\mu\text{T}$ . To further evaluate the signal stability, the data were magnified for the last 1 second duration, and a histogram with a mean 27  $\mu\text{T}$  and a standard deviation of about 1.5  $\mu\text{T}$  were extracted [Fig. 3(e)], indicating the practical magnetic field resolution of the system.

#### IV. DEPENDENCE OF THE MAGNETIC FIELD SENSING ON LASER AND MICROWAVE POWER

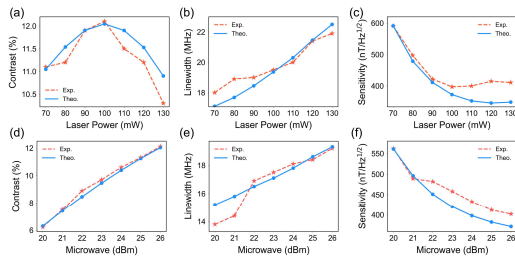


FIG. 4. Dependence of the magnetic field sensing

on the laser (a-c) and microwave power (d-f). The results are the PDMR contrast (a,d), linewidth (b,e) and the sensitivity estimated with Eq. (2) (c,f). Orange stars are the experimental data, and the blue dots are the results based on the master equation-based theory. In the panels (a-c), the microwave power is 26 dBm. In the panels (d-f), the laser power is 100 mW.

After demonstrating the PDMR-based magnetic field sensing, we examine now with Fig. 4 the dependence on the laser power (a-c) and the microwave power (d-f). Here, we set the lowest laser and microwave power as 70 mW and 20 dBm so that the PDMR spectrum can be faithfully determined, and the orange stars are the experimental data. As the laser power  $P$  increases from 70 mW to 130 mW, the contrast  $C$  increases firstly from 11.1%, approaches the maximum 12.1% for  $P = 100$  mW, and then decreases to 10.3% [Fig. 4(a)]. In contrast, the linewidth  $\Gamma$  increases mountainously from about 14.1 MHz to 21.9 MHz [Fig. 4(b)]. The behavior of the contrast can be understood through the competition of the optically induced spin polarization and the microwave absorption-induced population transfer, and the increased linewidth is caused by the increased rate of the former process [11,46,47]. Interestingly, the sensitivity  $\eta$  decreases fast from 600 nT/ $\sqrt{\text{Hz}}$  to about 400 nT/ $\sqrt{\text{Hz}}$  as the laser power increases from 70 mW to 100 mW, and then becomes saturated [Fig. 4(c)]. Based on Eq. (2), the flat feature can be understood by the cancelation of the quadratically increased carrier generation rate [Fig. S4(e)] to the increased ratio of the linewidth and contrast. In strong contrast, as the microwave power increases from 20 dBm to 26 dBm, the contrast increases from 6% to 12% [Fig. 4(d)], and the linewidth increases from 14 MHz to 20 MHz [Fig. 4(e)], which both can be attributed to the increased stimulated microwave absorption. As a result, the sensitivity shows a monotonous decay from 550 nT/ $\sqrt{\text{Hz}}$  to 400 nT/ $\sqrt{\text{Hz}}$  for increasing microwave power [Fig. 4(f)].

To understand further the experimental results, theoretical studies were carried out for the current system by adopting a quantum master equation to describe the processes of NV centers, as outlined in Fig. 1(b), using parameters reported in the previous literature and characterized with a commercial setup [48-50], see Section S4 of SM for more details. Furthermore, we have accounted for the number of NV centers  $2.551 \times 10^3$ , the conversion from the laser power to the optical pumping rate, and the conversion from the microwave power to the microwave magnetic field felt by the NV centers. The first parameter is estimated with the size of the laser focus and the NV concentration, and the second one is estimated from the laser power dependence of the fluorescence. Since the last parameter depends on the microwave field distribution and the relative position of the NV centers to the antenna, it is rather difficult to estimate and thus is considered as a fitting parameter. In the theoretical studies, we simulate the PDMR spectra to extract the contrast and linewidth, and then estimate the sensitivity according to Eq. (2). The theoretical results are presented by the blue dots in Fig. 4, and show a remarkable agreement with the experimental results.

Because of the good agreement with the experiment, the proposed theory can be further explored to optimize the PDMR device to achieve a better sensitivity. For example, by using an electron-irradiated diamond sample, the NV concentration can be increased by three orders of magnitude to few ppm. Then, the same orders of magnitude increase of the carriers detection rate might lead to an improvement of sensitivity by 32 times to tens  $\text{nT}/\sqrt{\text{Hz}}$  according to Eq. (2).

## V. CONCLUSIONS

In summary, we have carried out an experiment-theory joint study on the PDMR-based magnetic field sensing. By fabricating a diamond sample with electrodes and microwave antenna on the surface and using a

home-built setup, we obtain the PDMR spectrum by detecting photocurrent in nanoampere range with various lock-in amplifying modes. We have obtained a theoretically shot-noise limited sensitivity of  $397 \text{ nT}/\sqrt{\text{Hz}}$  with the laser power modulation mode, and an experimentally electronic noise-limited sensitivity  $921 \text{ nT}/\sqrt{\text{Hz}}$  with the microwave frequency-modulation mode. Importantly, for the first time, as far as we know, we demonstrate a real-time tracking of alternating magnetic field with a standard deviation of  $1.5 \mu\text{T}$ . To optimize the sensitivity further, we investigate systematically the dependence of the PDMR contrast, linewidth and the sensitivity on the laser and microwave power, and achieve a perfect agreement with a master equation-based model. Based on the model, we predict that the sensitivity can be improved by two orders of magnitude with an electron-irradiated diamond sample of higher NV concentration and a doubled voltage bias, reaching to tens  $\text{nT}/\sqrt{\text{Hz}}$ . This will be the direction pursued in the future, and paves the way for the the application of PDMR based quantum sensing.

## ACKNOWLEDGMENTS

This work was supported by the National Key R&D Program of China (Grant No. 2024YFE0105200), the Scientific Research Innovation Capability Support Project for Young Faculty (Grant No. SRICSPYF-BS2025008), the National Natural Science Foundation of China (Grant Nos. 62475242, 12422413, and U25A20192), the Joint Fund of Henan Province Science and Technology R&D Program (Grant No. 245200810005), the Cross disciplinary Innovative Research Group Project of Henan Province (Grant No. 232300421004). Xuan-Ming Shen carried out the results under the supervision of Yuan Zhang. All authors contributed to the analysis and writing of the manuscript.

**Conflict of interest** The authors declare that they have no conflict of interest.

## References

[1] J. Wrachtrup and F. Jelezko, Processing quantum information in diamond, *J. Phys.: Condens. Matter* **18**, S807 (2006).

[2] R. Katsumi, K. Takada, F. Jelezko and T. Yatsui, Recent progress in hybrid diamond photonics for quantum information processing and sensing, *Commun. Eng.* **4**, 85 (2025).

[3] S. Pezzagna and J. Meijer, Quantum computer based on color centers in diamond, *Appl. Phys. Rev.* **8**, 011308 (2021).

[4] G. Waldherr, Y. Wang, S. Zaiser, M. Jamali, T. Schulte-Herbrüggen, H. Abe, T. Ohshima, J. Isoya, J. F. Du, P. Neumann and J. Wrachtrup, Quantum error correction in a solid-state hybrid spin register, *Nature* **506**, 204 (2014).

[5] N. Kalb, A. A. Reiserer, P. C. Humphreys, J. J. W. Bakermans, S. J. Kamerling, N. H. Nickerson, S. C. Benjamin, D. J. Twitchen, M. Markham and R. Hanson, Entanglement distillation between solid-state quantum network nodes, *Science* **356**, 928 (2017).

[6] J. F. Barry, J. M. Schloss, E. Bauch, M. J. Turner, C. A. Hart, L.M. Pham and R. L. Walsworth, Sensitivity optimization for NV-diamond magnetometry, *Rev. Mod. Phys.* **92**, 015004 (2020).

[7] J. F. Du, F. Z. Shi, X. Kong, F. Jelezko and J. Wrachtrup, Single-molecule scale magnetic resonance spectroscopy using quantum diamond sensors, *Rev. Mod. Phys.* **96**, 025001 (2024).

[8] C. L. Degen, F. Reinhard and P. Cappellaro, Quantum sensing, *Rev. Mod. Phys.* **89**, 035002 (2017).

[9] N. Bar-Gill, L. M. Pham, A. Jarmola, D. Budke and R. L. Walsworth, Solid-state electronic spin coherence time approaching one second, *Nat. Commun.* **4**, 1743 (2013).

[10] S. Han, X. Ye, X. Zhou, Z. Liu, Y. Guo, M. Wang, W. Ji, Y. Wang and J. Du, Solid-state spin coherence time approaching the physical limit, *Sci. Adv.* **11**, eadr9298 (2025).

[11] E. Bourgeois, J. Soucek, J. Hruby, M. Gulka and M. Nesladek, Photoelectric Detection of Nitrogen-Vacancy Centers Magnetic Resonances in Diamond: Role of Charge Exchanges with Other Optoelectrically Active Defects, *Adv. Quantum Technol.* **5**, 2100153 (2022).

[12] V. M. Acosta, E. Bauch, A. Jarmola, L. J. Zipp, M. P. Ledbetter and D. Budker, Broadband magnetometry by infrared-absorption detection of nitrogen-vacancy ensembles in diamond, *Appl. Phys. Lett.* **97**, 174104 (2010).

[13] E. R. Eisenach, J. F. Barry, M. F. O'Keeffe, J. M. Schloss, M. H. Steinecker, D. R. Englund and D. A. Braje, Cavity-enhanced microwave readout of a solid-state spin sensor, *Nat. Commun.* **12**, 1357 (2021).

[14] F. M. Hrubesch, G. Braunbeck, M. Stutzmann, F. Reinhard and M. S. Brandt, Efficient Electrical Spin Readout of NV<sup>-</sup> Centers in Diamond, *Phys. Rev. Lett.* **118**, 037601 (2017).

[15] E. Bourgeois, A. Jarmola, P. Siyushev, M. Gulka, J. Hruby, F. Jelezko, D. Budker and M. Nesladek, Photoelectric detection of electron spin resonance of nitrogen-vacancy centres in diamond, *Nat. Commun.* **6**, 8577 (2015).

[16] E. Bourgeois, M. Gulka and M. Nesladek, Photoelectric Detection and Quantum Readout of Nitrogen-Vacancy Center Spin States in Diamond, *Adv. Optical Mater.* **8**, 1902132 (2020).

[17] T. Murooka, M. Shiigai, Y. Hironaka, T. Tsuji, B. Yang, T. M. Hoang, K. Suda, K. Mizuno, H. Kato, T. Makino, M. Ogura, S. Yamasaki, M. Hatano and T. Iwasaki, Photoelectrical detection of nitrogen-vacancy centers by utilizing diamond lateral p-i-n diodes, *Appl. Phys. Lett.* **118**, 253502 (2021).

[18] H. Morishita, N. Morioka, T. Nishikawa, H. Yao, S. Onoda, H. Abe, T. Ohshima and N. Mizuochi, Spin-Dependent Dynamics of

Photocarrier Generation in Electrically Detected Nitrogen-Vacancy-Based Quantum Sensing, *Phys. Rev. Appl.* **19**, 034061 (2023).

[19] L. M. Todenhagen and M. S. Brandt, Optical and electrical readout of diamond NV centers in dependence of the excitation wavelength, *Appl. Phys. Lett.* **126**, 194003 (2025).

[20] D. Wirtitsch, G. Wachter, S. Reisenbauer, J. Schalko, U. Schmid, A. Fant, L. Sant and M. Trupke, Microelectronic readout of a diamond quantum sensor, arXiv:2403.0309.

[21] M. Gulka, E. Bourgeois, J. Hruby, P. Siyushev, G. Wachter, F. Aumayr, P. R. Hemmer, A. Gali, F. Jelezko, M. Trupke and M. Nesladek, Pulsed Photoelectric Coherent Manipulation and Detection of N–V Center Spins in Diamond, *Phys. Rev. Appl.* **7**, 044032 (2017).

[22] E. Bourgeois, E. Londero, K. Buczak, J. Hruby, M. Gulka, Y. Balasubramaniam, G. Wachter, J. Stursa, K. Dobes, F. Aumayr, M. Trupke, A. Gali and M. Nesladek, Enhanced photoelectric detection of NV magnetic resonances in diamond under dual-beam excitation, *Phys. Rev. B* **95**, 041402 (2017).

[23] P. Siyushev, M. Nesladek, E. Bourgeois, M. Gulka, J. Hruby, T. Yamamoto, M. Trupke, T. Teraji, J. Isoya and F. Jelezko, Photoelectrical imaging and coherent spin-state readout of single nitrogen-vacancy centers in diamond, *Science* **363**, 728 (2019).

[24] S. Nakamura, N. Morioka, N. Mizuochi, S. Mizukami and H. Morishita, Scanning photocurrent imaging resolution of single NV center in diamond, *Appl. Phys. Lett.* **2** 127 (2025).

[25] H. Morishita, S. Kobayashi, M. Fujiwara, H. Kato, T. Makino, S. Yamasaki and N. Mizuochi, Room Temperature Electrically Detected Nuclear Spin Coherence of NV Centres in Diamond, *Sci. Rep.* **10**, 792 (2020).

[26] M. Gulka, D. Wirtitsch, V. Ivády, J. Vodnik, J. Hruby, G. Magchiels, E. Bourgeois, A. Gali, M. Trupke and M. Nesladek, Room-temperature control and electrical readout of individual nitrogen-vacancy nuclear spins, *Nat. Commun.* **12**, 4421 (2021).

[27] N. Aslam, G. Waldherr, P. Neumann, F. Jelezko and J. Wrachtrup, Photo-induced ionization dynamics of the nitrogen vacancy defect in diamond investigated by single-shot charge state detection, *New J. Phys.* **15**, 13064 (2013).

[28] J. Hruby, M. Gulka, M. Mongillo, I. P. Radu, M. V. Petrov, E. Bourgeois and M. Nesladek, Magnetic field sensitivity of the photoelectrically read nitrogen-vacancy centers in diamond, *Appl. Phys. Lett.* **120**, 162402 (2022).

[29] H. Zheng, J. Hruby, E. Bourgeois, J. Soucek, P. Siyushev, F. Jelezko, A. Wickenbrock, M. Nesladek and D. Budker, Electrical-Readout Microwave-Free Sensing with Diamond, *Phys. Rev. Appl.* **18**, 24079 (2022).

[30] M. Niethammer, M. Widmann, T. Rendler, N. Morioka, Y. C. Chen, R. Stöhr, J. U. Hassan, S. Onoda, T. Ohshima, S. Y. Lee, A. Mukherjee, J. Isoya, N. T. Son and J. Wrachtrup, Coherent electrical readout of defect spins in silicon carbide by photo-ionization at ambient conditions, *Nat. Commun.* **10**, 5569 (2019).

[31] T. Nishikawa, N. Morioka, H. Abe, K. Murata, K. Okajima, T. Ohshima, H. Tsuchida and N. Mizuochi, Coherent photoelectrical readout of single spins in silicon carbide at room temperature, *Nat. Commun.* **16**, 3405 (2025).

[32] S. Ru, L. An, H. Liang, Z. Jiang, Z. Li, X. Lyu, F. Zhou, H. Cai, Y. Yang, R. He, R. Cernansky, E. H. T. Teo, M. Mukherjee, A. A. Bettoli, J. Zúñiga-Perez, F. Jelezko and Weibo Gao, Room-Temperature Electrical Readout of Spin Defects in van der Waals Materials, *Phys. Rev. Lett.* **135**, 220802 (2025).

[33] N. Sekiguchi, M. Fushimi, A. Yoshimura, C.

Shinei, M. Miyakawa, T. Taniguchi, T. Teraji, H. Abe, S. Onoda, T. Ohshima, M. Hatano, M. Sekino and T. Iwasaki, Diamond quantum magnetometer with dc sensitivity of sub-10 pT Hz<sup>-1/2</sup> toward measurement of biomagnetic field, *Phys. Rev. Appl.* **21**, 064010 (2024).

[34] S. Ahmadi, H. A. R. El-Ella, J. O. B. Hansen, A. Huck and U. L. Andersen, Pump-Enhanced Continuous-Wave Magnetometry Using Nitrogen-Vacancy Ensembles, *Phys. Rev. Appl.* **8**, 034001 (2017).

[35] S.-C. Zhang, Y. Dong, B. Du, H.-B. Lin, S. Li, W. Zhu, G.-Z. Wang, X.-D. Chen, G.-C. Guo and F.-W. Sun, A robust fiber-based quantum thermometer coupled with nitrogen-vacancy centers, *Rev. Sci. Instrum.* **92**, 044904 (2021).

[36] J. Zhang, T. Liu, L. Xu, G. Bian, P. Fan, M. Li, C. Xu and H. Yuan, A pulsed lock-in method for DC ensemble nitrogen-vacancy center magnetometry, *Diam. Relat. Mater.* **125**, 109035 (2022).

[37] S. Johansson, D. Lönard, I. C. Barbosa, J. Gutsche, J. Witzenrath and A. Widera, Miniaturized magnetic-field sensor based on nitrogen-vacancy centers, *Phys. Rev. Appl.* **24**, 054078 (2025).

[38] C.-N. Lin, Z.-F. Zhang, Y.-J. Lu, X. Yang, Y. Zhang, X. Li, J.-H. Zang, X.-C. Pang, L. Dong and C.-X. Shan, High performance diamond-based solar-blind photodetectors enabled by Schottky barrier modulation, *Carbon* **200**, 510 (2022).

[39] X. P. Le, L. Mayer, S. Magaletti, M. Schmidt, J.-F. Roch and T. Debuisschert, Field-effect detected magnetic resonance of nitrogen-vacancy centers in diamond based on all-carbon Schottky contacts, *Commun. Eng.* **4**, 209 (2025).

[40] A. Dréau, M. Lesik, L. Rondin, P. Spinicelli, O. Arcizet, J.-F. Roch and V. Jacques, Avoiding power broadening in optically detected magnetic resonance of single NV defects for enhanced dc magnetic field sensitivity, *Phys. Rev. B* **84**, 195204 (2011).

[41] J. J. Moré, in *Numerical Analysis*, Vol. 630, edited by G. A. Watson (Springer Berlin Heidelberg, Berlin, Heidelberg, 1978), p. 105, series Title: Lecture Notes in Mathematics.

[42] J. M. Schloss, J. F. Barry, M. J. Turner and R. L. Walsworth, Simultaneous Broadband Vector Magnetometry Using Solid-State Spins, *Phys. Rev. Appl.* **10**, 034044 (2018).

[43] J. L. Webb, J. D. Clement, L. Troise, S. Ahmadi, G. J. Johansen, A. Huck and U. L. Andersen, Nanotesla sensitivity magnetic field sensing using a compact diamond nitrogen-vacancy magnetometer, *Appl. Phys. Lett.* **114**, 231103 (2019).

[44] D. A. Van Baak and G. Herold, Response of a lock-in amplifier to noise, *Am. J. Phys.* **82**, 785(2014).

[45] R. L. Patel, L. Q. Zhou, A. C. Frangeskou, G. A. Stimpson, B. G. Breeze, A. Nikitin, M. W. Dale, E. C. Nichols, W. Thornley, B. L. Green, M. E. Newton, A. M. Edmonds, M. L. Markham, D. J. Twitchen and G. W. Morley, Subnanotesla Magnetometry with a Fiber-Coupled Diamond Sensor, *Phys. Rev. Appl.* **14**, 044058 (2020).

[46] K. Jensen, V. M. Acosta, A. Jarmola and D. Budker, Light narrowing of magnetic resonances in ensembles of nitrogen-vacancy centers in diamond, *Phys. Rev. B* **87**, 014115 (2013).

[47] J. Soucek, M. Petrov, M. Gulka, E. Bourgeois and M. Nesladek, Modelling and experimental verification of photoelectrical response of NV diamond spin centres, arXiv:2511.19583v2.

[48] K.-M. C. Fu, C. Santori, P. E. Barclay, L. J. Rogers, N. B. Manson and R. G. Beausoleil, Observation of the Dynamic Jahn-Teller Effect in the Excited States of Nitrogen-Vacancy Centers in Diamond, *Phys. Rev. Lett.* **103**, 256404 (2009).

[49] B. Julsgaard and K. Mølmer, Dynamical evolution of an inverted spin ensemble in a cavity: Inhomogeneous broadening as a stabilizing mechanism, *Phys. Rev. A* **86**, 63810 (2012).

[50] M. Pallmann, K. Köster, Y. Zhang, J. Heupel, T. Eichhorn, C. Popov, K. Mølmer and D. Hunger, Cavity-mediated collective emission from few emitters in a diamond membrane, *Phys. Rev. X* **14**, 041055 (2024).